

Accepted Article Preview: Published ahead of advance online publication

This is a PDF file of an unedited peer-reviewed manuscript that has been accepted for publication. The manuscript will undergo copyediting, typesetting and a proof review before it is published in its final form. Please note that during the production process errors may be discovered which could affect the content, and all legal disclaimers apply.

Perfect electromagnetic and sound absorption via subwavelength holes array

Journal:	Opto-Electronic Advances
Manuscript ID:	oea-2018-0013
Manuscript type:	Original Article
List of Authors:	Yanqin Wang; Institute of Optics and Electronics, CAS, Xiaoliang Ma; Institute of Optics and Electronics, CAS, Xiong Li; Institute of Optics and Electronics, CAS, Mingbo Pu; Institute of Optics and Electronics, CAS, Xiangang Luo; Institute of Optics and Electronics, CAS,
Keywords:	metasurface; absorber
Speciality:	Metasurface
DOI:	10.29026/oea.2018.180013
Cite this article as:	Wang Y Q, Ma X L, Li X, Pu M B, Luo X G. Perfect electromagnetic and sound absorption via subwavelength holes array. <i>Opto-Electronic Advances</i> 1 , 180013 (2018).
Received 11-Aug-2018 ; accepted 30-Aug-2018; Accepted article preview online 13-Sep-2018	

SCHOLARONE™
Manuscripts

Perfect electromagnetic and sound absorption via subwavelength holes array

Yanqin Wang, Xiaoliang Ma, Xiong Li,

Mingbo Pu and Xiangang Luo*

State Key Laboratory of Optical Technologies on Nano-Fabrication and Micro-Engineering, Institute of Optics and Electronics,
Chinese Academy of Sciences, Chengdu, 610209, China

* Correspondence: X G Luo, Email: lxg@ioe.ac.cn

Abstract: Broadband sound absorption at low frequency is notoriously difficult because the thickness of the absorber should be proportional to the working wavelength. Here we report an acoustic metasurface absorber following the recent theory developed for electromagnetics. We first show that there is an intrinsic analogy between the impedance description of sound and electromagnetic metasurfaces. Subsequently, we demonstrated that the classic Salisbury and Jaumann absorbers can be realized for acoustic applications with the aid of micro-perforated plates. Finally, the concept of coherent perfect absorption is introduced to achieve ultrathin and ultra-broadband sound absorbers. We anticipate that the approach proposed here can provide helpful guidance for the design of future acoustic and electromagnetic devices.

Keywords: metasurface; absorber

Introduction

Perhaps all things around us are some types of waves, such as the light waves, acoustic waves, matter waves and even gravitational waves. The absorption or dissipation of the energy carried by these waves are of great importance in many applications ranging from energy harvest and information exchange to radar wave and sound noise control¹⁻⁸. Among the various types of waves, the electromagnetic and acoustic waves shared many similarities. In the last decades, the two disciplines have borrowed concepts from each other to grow up alternately. For example, the time-reversed sub-diffraction focusing technique was first developed by the acousticians and then utilized in the optical domain to break the diffraction limit⁹⁻¹². On the other hand, the hyperlens was originally created in the optical domain and then introduced to acoustic research^{13,14}. Recently, the concept of metasurface, an artificially structured thin film with property on demand, has become a hot spot in both the electromagnetic and acoustic regimes¹⁵⁻¹⁸. It is, however, surprising that many metasurface concepts such as Salisbury and Jaumann absorbers in the electromagnetic design have not been extended into the acoustic domain. Furthermore, although ultrathin and ultra-broadband electromagnetic absorbers have been realized^{19,20}, similar thin absorbers are still difficult to obtain for acousticians^{4,17}.

In this paper, we theoretically compared the boundary conditions for electromagnetic and acoustic metasurfaces. Similar to electromagnetic metasurface absorber, we show that various acoustic absorbers can be achieved using the effective impedance of deep-subwavelength perforated rigid plate (may be approximated by steel). In particular, an ultra-broadband and thin acoustic perfect absorber is demonstrated under coherent condition, showing excellent performance comparable to its electromagnetic counterpart.

Results

Analogy between the boundary conditions of electromagnetic and acoustic waves.

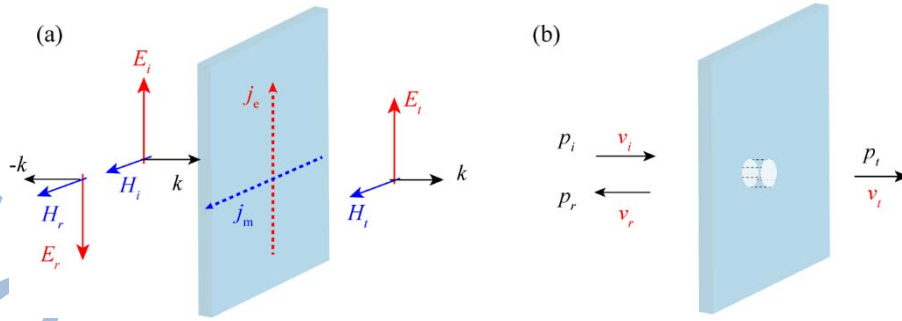


Fig. 1 | Boundary conditions for the electromagnetic and acoustic waves on a thin plate. (a) Electric and magnetic fields matching. (b) Pressure and velocity matching.

First of all, the boundary conditions for electromagnetic metasurface are considered. As shown in Fig. 1a, the tangential components of the electric and magnetic fields are continuous at the interface between two half-infinite materials. When a non-magnetic impedance sheet with zero thickness is placed at this interface²¹, the boundary conditions should be rewritten as

$$\begin{aligned} \vec{E}_{t,\parallel} + \vec{E}_{r,\parallel} &= \vec{E}_{t,\parallel} \\ \vec{H}_{i,\parallel} + \vec{H}_{r,\parallel} &= \vec{H}_{t,\parallel} + \hat{n} \times Y_{s,em} \vec{E}_{t,\parallel} \end{aligned} \quad (1)$$

where i , r and t denote the incidence, reflection and transmission, \parallel represents the tangential components, \hat{n} is the unit vector along the normal direction, $Y_{s,em}$ is the electric sheet inductance of the metasurface.

Since \vec{E} and \vec{H} are related via the Faraday's law,

$$\nabla \times E = -\mu \frac{\partial H}{\partial t} \quad (2)$$

equation (1) can be reduced to be

$$\begin{aligned} 1 + r_{em} &= t_{em} \\ Y_{1,em} (1 - r_{em}) &= Y_{2,em} t_{em} + Y_{s,em} t_{em} \end{aligned} \quad (3)$$

where r_{em} and t_{em} are the reflection and transmission coefficients defined by the electric fields, $Y_{1,em}$ are $Y_{2,em}$ are the inductances of two materials in the left and right sides.

Similar to the electromagnetic case, the boundary conditions for an acoustic impedance sheet (Fig. 1b) has the form of

$$v_{i,\perp} + v_{r,\perp} = v_{t,\perp} \quad (4)$$

and

$$p_i + p_r = p_t + Z_{s,ac} v_{t,\perp} \quad (5)$$

where v and p are the velocity and pressure of the sound perturbation. While equation (4) is a direct result of the mass conservation, equation (5) is obtained by defining the effective sheet impedance

$$Z_{s,ac} = \frac{p_i + p_r - p_t}{v_{t,\perp}} = \frac{\Delta p}{\bar{v}_{\perp}} \quad (6)$$

In general, v and p are related through the characteristic impedance

$$\begin{aligned} p_i &= Z_{1,ac} v_{i,\perp} \\ p_r &= Z_{1,ac} v_{r,\perp} \\ p_t &= Z_{2,ac} v_{t,\perp} \end{aligned} \quad (7)$$

Assuming that the background is filled with air, the impedance can be written as $Z_{1,ac} = Z_{2,ac} = \rho c / \cos \theta$, where θ is the incidence angle, c is the velocity of acoustic wave. Combing equations (4)-(7), one can obtain the following expression

$$\begin{aligned} 1 + r_{ac} &= t_{ac} \\ Z_{1,ac} (1 - r_{ac}) &= Z_{2,ac} t_{ac} + Z_{s,ac} t_{ac} \end{aligned} \quad (8)$$

Interestingly, equations (3) and (8) have very similar form, except that the admittance in equation (3) is replaced by the impedance in equation (8). This similarity implies that both the acoustic and electromagnetic problems in metasurfaces can be solved by transfer matrix, along with proper boundary conditions.

Impedance sheet realized by micro-perforated plate

In the above discussion, an arbitrary sheet impedance is assumed without considering its practical realization. In the following, the effective impedance of micro-perforated plate (MPP) is utilized in the design of various acoustic absorbers. It should be noted that although the MPP absorbers have been intensively studied after its invention by Maa in 1970s²²⁻²⁴, its intrinsic similarity with electromagnetic absorber such as Salisbury and Jaumann absorbers has seldom been studied²⁵⁻²⁷. In this paper, we show that the concept borrowed from electromagnetics is very efficient in the design of acoustic devices.

In general, the effective impedance of a micro-tube perforated in a rigid plate should be calculated using computational fluid dynamics (CFD)²³. However, when the tube is short compared to the wavelength, the effective impedance can be approximately analyzed using the equation of aerial motion

$$i\omega\rho_0 v - \frac{\eta}{r_1} \frac{\partial}{\partial r_1} \left(r_1 \frac{\partial}{\partial r_1} v \right) = \frac{\Delta p}{t}, \quad (9)$$

where v is particle velocity, $\omega = 2\pi f$ the angular frequency, Δp the sound pressure between the ends of the tube, t the thickness of the tube (equal to that of the panel), ρ_0 the density of air, η the coefficient of viscosity, and r_1 the radius vector of cylindrical coordinates inside the tube. The specific acoustic impedance can be obtained as

$$Z_{tube} = \frac{\Delta p}{\bar{v}} = i\omega\rho_0 t \left[1 - \frac{2}{k\sqrt{-i}} \frac{J_1(\kappa\sqrt{-i})}{J_0(\kappa\sqrt{-i})} \right]^{-1}, \quad (10)$$

where $\kappa = r_0 \sqrt{\rho_0 \omega / \eta}$ is the perforate constant, r_0 is the radius of the tube, J_1 the Bessel function of the first kind, J_0 the Bessel function of zeroth kind. The normalized impedance can be obtained as

$$Z_{s,ac} = \frac{Z_{tube}}{\sigma} \quad (11)$$

where $\sigma = \frac{A_{hole}}{A_{cell}}$ is the perforation ratio in area. In practical applications, the hole's dynamic end correction should be considered, leading to the following sheet impedance

$$Z_s = \frac{t + \beta d}{t} Z_{s,ac}, \quad (12)$$

where $\beta = 0.613$ is an empirical parameter²³.

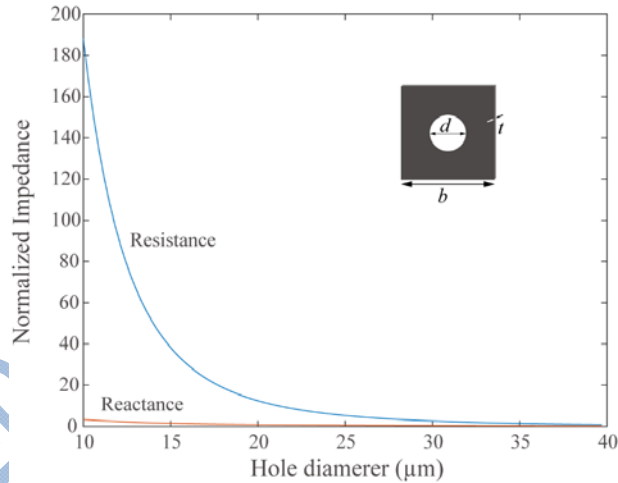


Fig. 2 | Normalized impedance versus the hole diameter (d) at a frequency of 10 kHz. $b = t = 100 \mu\text{m}$.

The normalized impedance at $f = 10$ kHz for different hole diameters is plotted in Fig. 2. Clearly, as the increase of the hole diameter, the impedance drops down rapidly. When the hole is extremely small, the impedance tends to be infinite, with all sound wave being reflected. The frequency-dependent impedance of a MPP metasurface is shown in Fig. 3, where the geometric parameters are fixed as $d = 38.5 \mu\text{m}$ and $b = t = 100 \mu\text{m}$. Evidently, the resistance is almost independent of the frequency, while the reactance is proportional to the frequency.

From above results, it is clear that a thin micro-perforated plate bear similar properties with the resistive sheet (thin metal film) in the electromagnetic applications²⁵. Combining with the similarity in boundary conditions, it can be concluded that the acoustic waves can be controlled using electromagnetic-inspired approaches. Furthermore, it is expected that more complex sheet impedance is possible by combing the micro-perforated plate with cavities or other resonant structures²⁸.

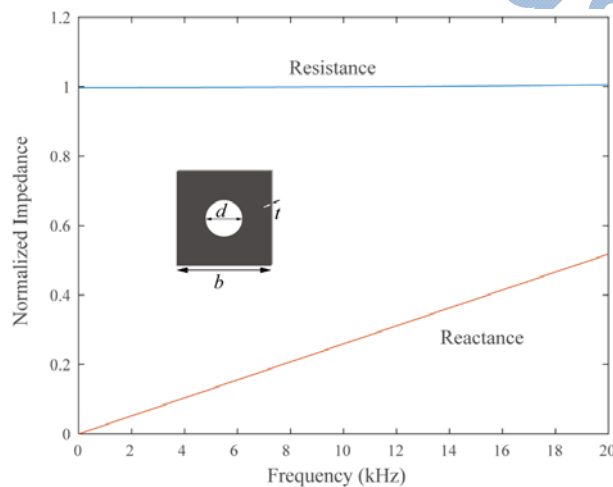


Fig. 3 | Normalized impedance of micro-perforated plate. $d = 38.5 \mu\text{m}$, $b = t = 100 \mu\text{m}$.

Acoustic Salisbury and Jaumann absorbers

As the first step to demonstrate the intrinsic connection between the electromagnetic and acoustic metasurface, the acoustic-type Salisbury^{25,29} and Jaumann³⁰ absorbers are investigated. As depicted in Fig. 4, the absorption spectra of two optimized absorbers are calculated using transfer matrix method (see methods). Theoretically, the physical mechanism behind the absorption is the multiple interference between successive reflections³¹. Although only theoretical results are given here, previous experiments agree well with our theory²⁴, indicating that the following discussion is sound and robust.

For the Salisbury-type absorber, there is only one micro-perforated plate (labelled as MPP-1) separated from the rigid body with a distance of $h_1 = 48$ mm. The geometric parameters of MPP-1 is $d_1 = 38.5 \mu\text{m}$ and $b = t = 100 \mu\text{m}$. For the Jaumann-type absorber, there are four MPPs placed successively with distance $h_1 = h_2 = h_3 = h_4 = 12$ mm. The thickness t and period b are equal for all these MPPs, while the hole diameters are $d_1 = 38.5 \mu\text{m}$, $d_2 = 40 \mu\text{m}$, $d_3 = 45 \mu\text{m}$ and $d_4 = 50 \mu\text{m}$. Note that the one-layer Salisbury and four-layer Jaumann structures are two representing examples. For the two- and three-layer structures, the bandwidth would be larger than the one-layer but smaller than the four-layer cases. Similar to the electromagnetic case, the thickness mainly determines the absorption frequency. As the thickness becomes larger, the frequency will become smaller.

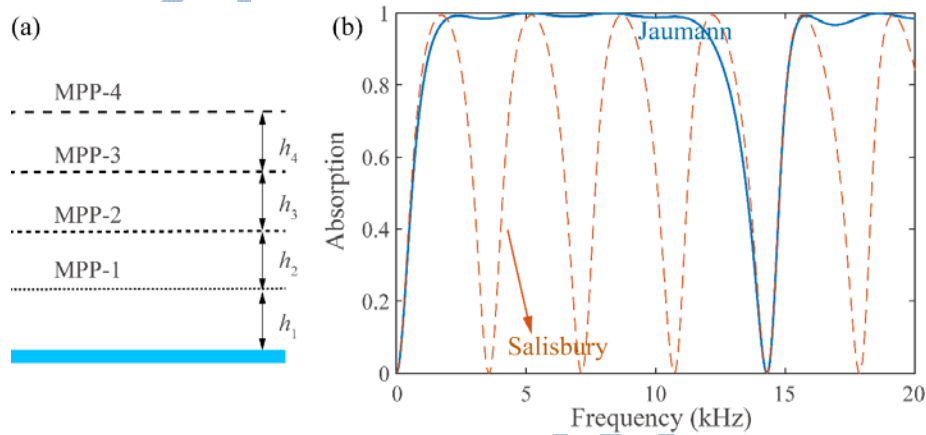


Fig. 4 | Acoustic Salisbury and Jaumann absorbers. (a) Schematic of the configuration of the multilayered acoustic absorbers. (b) Absorption spectra of the acoustic Salisbury and Jaumann absorbers.

As illustrated in Fig. 5, the dependence of the acoustic Jaumann absorber on the incidence angle θ is also investigated. Similar to its electromagnetic counterpart, the absorption efficiency would decrease as the rise of the incidence angle although most is larger than 90% for $\theta < 60^\circ$. In addition, we noted that the angle dependence is similar to the transverse electric (TE) mode, rather than the transverse magnetic (TM) mode, as can be derived from the boundary conditions.

Anyway, the results shown in Figs. 4 and 5 resemble that for classic electromagnetic absorbers¹. Consequently, we expect that the theory of the recent developed electromagnetic absorbers^{3,32} can be leveraged to design acoustic absorbers in a more sophisticated way.

Opto-Electronic Advances

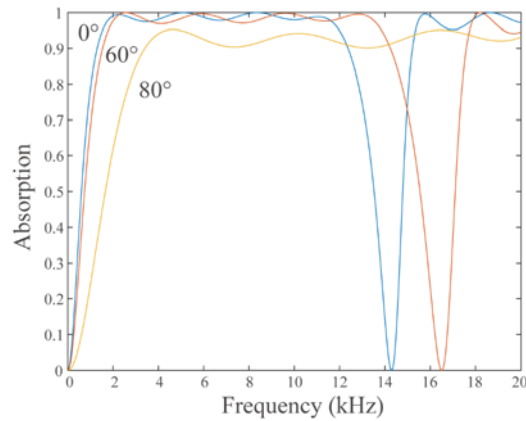


Fig. 5 | Angular dependence of the Jaumann absorber. As the incidence angle is increased from the 0° to 80° , the absorption valley position at about 14 kHz shifts to higher frequencies, accompanying with a small decrease of the absorption efficiency.

Coherent perfect absorption of acoustic wave

Different from traditional absorbers, coherent perfect absorption (CPA) is a process that requires two or more coherent inputs^{19,20,33–37}. Owing to the revision of the operation condition, previous limitation on the bandwidth and absorber thickness, as set by the causality and Kramers-Kronig relations³⁸, can be eliminated^{19,39}. This broadband coherent absorption characteristic seems a surprise since CPA was thought as a time-reversed process of lasing, which is intrinsically narrowband⁴⁰. Nevertheless, from the view point of electrodynamics, this broadband absorption can be indeed treated as the time-reversed process of the radiating current sheet¹⁹, which is not limited in bandwidth. Although CPA is of particular importance for electromagnetic applications, its realization in acoustic region is hampered by the absence of proper lossy materials¹⁷. Although there are some attempts to design acoustic CPA⁴¹, the results seems not so satisfactory because only narrowband absorption can be achieved.

Figure 6 illustrated the absorption spectrum under CPA condition. The hole diameter of the MPP is $32.1 \mu\text{m}$, while the thickness and period are both $100 \mu\text{m}$. As we expected, the absorption can be as high as 99% at frequencies below 10 kHz, which is very similar to the ultra-broadband electromagnetic CPA¹⁹. It should be noted that the normalized impedance for the MPP at CPA condition is nearly twice that of air, while in the electromagnetic case the impedance is only half. This difference is a direct result of the different definition of impedance in acoustics and electromagnetics. Furthermore, since the amplitude of the acoustic wave is defined using the pressure p , the CPA condition requires $s = -1$ (asymmetric mode), which is also contrary to the electromagnetic CPA¹⁹.

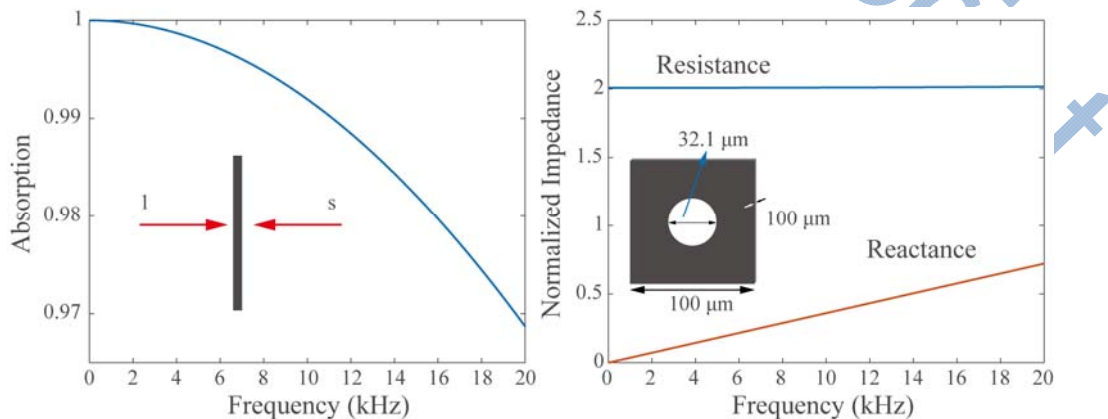


Fig. 6 | Acoustic coherent perfect absorber. (a) Absorption spectra of the coherent perfect absorber. (b) Normalized impedance at different frequencies.

One of the intrinsic advantages of CPA over traditional absorbers lies in the fact that the absorption can be easily tuned by varying the phase difference between the left and right inputs (l). Similar to the electromagnetic counterpart¹⁹, the absorption may be written as:

$$A = 1 - \sin^2\left(\frac{\omega l}{2v_0}\right) \quad (13)$$

where $v_0 = 343$ m/s is the velocity of sound in air.

As shown in Fig. 7(a), when the path difference is fixed to be 0.2 m, the absorption spectra vary rapidly with the sound frequency. Note that the absorption at very low frequency is always near 100%, implying that this technique is very efficient for the absorption at low frequency. Figure 7b depicts the absorption at 10 kHz for various path difference, where the ratio of the minimum to maximum can be as smaller as $2e-5$, which is beneficial to the coherent acoustic modulators. Similar to the concept of “controlling light with light”⁴², the acoustic CPA can be also leveraged to realize “controlling sound with sound” on metasurfaces.

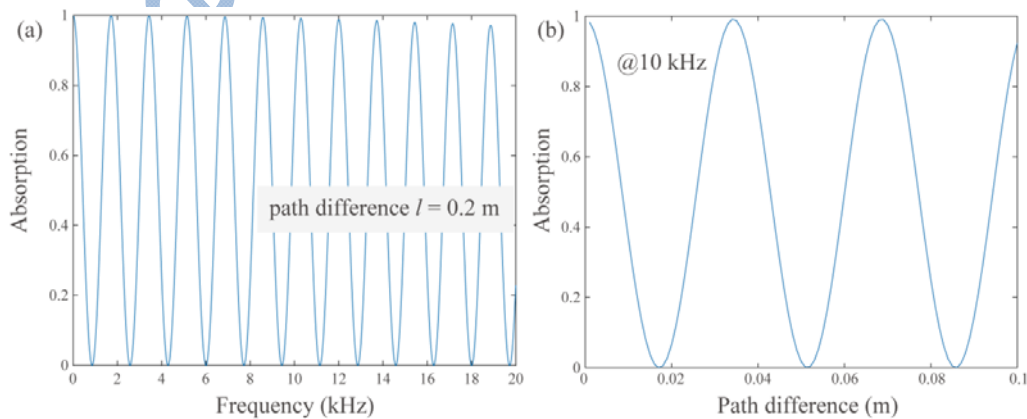


Fig. 7 | Variation in the absorption under different coherent conditions.

(a) Absorption versus frequency f with path difference of $l = 0.2$ m. (b) Absorption versus l at $f = 10$ kHz.

Discussions

In summary, we have unified the theory of electromagnetic and acoustic absorbers in the context of metasurfaces. It is demonstrated unambiguously that the theory of electromagnetic absorbers can provide useful guidance for acoustic researches. The ultra-broadband acoustic CPA proves that previous judgment about sound absorption, especially at low frequency, is not accurate¹⁷.

It should be pointed out that the impedance of the MPP is mainly determined by the radius of the deep-subwavelength-scale holes, which are also of particular importance in electromagnetic scenarios such as the extraordinary optical transmission⁴³ and frequency selective surfaces⁴⁴. As the operational frequency rises, the holes need to be scaled down to maintain the required impedance and there will be huge challenges to fabricate such small holes in a large area. Meanwhile, the accuracy of Maa’s model needs further experimental investigation at higher frequency. Nevertheless, there is no problem if we focus on the low-frequency regime, which is just the difficult point of traditional approaches. Potential applications may be found in the noise control in both air and water environments.

Method of transfer matrix for the multilayered acoustic absorber

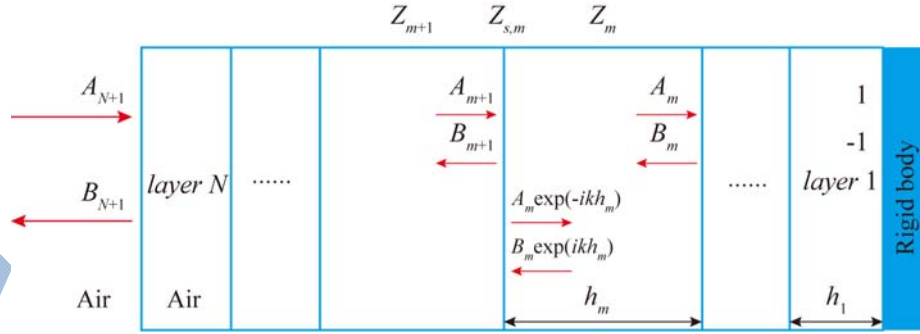


Fig. 8 | Schematic of the acoustic multilayer. In each layer, there are two counter-propagating waves with amplitudes of A and B . These amplitudes are connected with matrix shown in the text.

Similar to the electromagnetic case, the multilayered acoustic structure can be calculated efficiently using the transfer matrix. As depicted in Fig. 8, the coefficients of the counter-propagating acoustic waves are denoted as A and B , while the two pairs of quantities can be written as

$$\begin{bmatrix} A_{m+1} \\ B_{m+1} \end{bmatrix} = \frac{1}{2Z_{m+1}} \begin{bmatrix} Z_{m+1} + Z_m + Z_{s,m} & Z_{m+1} - Z_m + Z_{s,m} \\ Z_{m+1} - Z_m - Z_{s,m} & Z_0 + Z_1 - Z_{s,m} \end{bmatrix} \begin{bmatrix} \exp(-ikh_m) & 0 \\ 0 & \exp(ikh_m) \end{bmatrix} \begin{bmatrix} A_m \\ B_m \end{bmatrix}, \quad (14)$$

where

$$M_{1,m} = \frac{1}{2Z_{m+1}} \begin{bmatrix} Z_{m+1} + Z_m + Z_{s,m} & Z_{m+1} - Z_m + Z_{s,m} \\ Z_{m+1} - Z_m - Z_{s,m} & Z_0 + Z_1 - Z_{s,m} \end{bmatrix} \quad (15)$$

is the transition matrix of the metasurface, while

$$M_{2,m} = \begin{bmatrix} \exp(-ikh_m) & 0 \\ 0 & \exp(ikh_m) \end{bmatrix} \quad (16)$$

is the propagation matrix of the m^{th} layer. Here $k = \cos(\theta)\omega / c$ is the normal component of the acoustic wave number.

Obviously, the amplitudes of acoustic waves at the outmost layer can be calculated from the innermost directly. Since there is a rigid body acting as a perfect reflector, the final form of the transfer matrix can be written as

$$\begin{bmatrix} A_{N+1} \\ B_{N+1} \end{bmatrix} = M_N M_{N-1} \cdots M_2 M_1 \begin{bmatrix} 1 \\ -1 \end{bmatrix} \quad (17)$$

where $M_m = M_{1,m} M_{2,m}$ is the transfer matrix of a pair of air and metasurface. The reflection and absorption coefficients can be then calculated as

$$Reflection = \frac{B_{N+1}}{A_{N+1}} \quad (18)$$

and

$$Absorption = 1 - \left(\frac{B_{N+1}}{A_{N+1}} \right)^2 \quad (19)$$

References

1. Knott E F, Shaeffer J F, Tuley M T. *Radar Cross Section* 2nd ed (SciTech Publishing, Raleigh, North Carolina, 2004).
2. Hao J M, Wang J, Liu X L, Padilla W J, Zhou L *et al.* High performance optical absorber based on a plasmonic metamaterial. *Appl Phys Lett* **96**, 251104 (2010).
3. Feng Q, Pu M B, Hu C G, Luo X G. Engineering the dispersion of metamaterial surface for broadband infrared absorption. *Opt Lett* **37**, 2133–2135 (2012).
4. Mei J, Ma G C, Yang M, Yang Z Y, Wen W J *et al.* Dark acoustic metamaterials as super absorbers for low-frequency sound. *Nat Commun* **3**, 756 (2012).
5. Vora A, Gwamuri J, Pala N, Kulkarni A, Pearce J M *et al.* Exchanging ohmic losses in metamaterial absorbers with useful optical absorption for photovoltaics. *Sci Rep* **4**, 4901 (2014).
6. Song M W, Yu H L, Hu C G, Pu M B, Zhang Z J *et al.* Conversion of broadband energy to narrowband emission through double-sided metamaterials. *Opt Express* **21**, 32207–32216 (2013).
7. Cui Y X, He Y R, Jin Y, Ding F, Yang L *et al.* Plasmonic and metamaterial structures as electromagnetic absorbers. *Laser Photonics Rev* **8**, 495–520 (2014).
8. Luo X G. Principles of electromagnetic waves in metasurfaces. *Sci China Phys Mech Astron* **58**, 594201 (2015).
9. de Rosny J, Fink M. Overcoming the diffraction limit in wave physics using a time-reversal mirror and a novel acoustic sink. *Phys Rev Lett* **89**, 124301 (2002).
10. Lerosey G, de Rosny J, Tourin A, Fink M. Focusing beyond the diffraction limit with far-field time reversal. *Science* **315**, 1120–1122 (2007).
11. Chen L W, Zhou Y, Wu M X, Hong M H. Remote-mode microsphere nano-imaging: new boundaries for optical microscopes. *Opto-Electron Adv* **1**, 170001 (2018).
12. Qin F, Hong M H. Breaking the diffraction limit in far field by planar metalens. *Sci China Phys Mech Astron* **60**, 044231 (2017).
13. Jacob Z, Alekseyev L V, Narimanov E. *Optical hyperlens: Far-field imaging beyond the diffraction limit.* *Opt Express* **14**, 8247–8256 (2006).
14. Li J, Fok L, Yin X B, Bartal G, Zhang X. Experimental demonstration of an acoustic magnifying hyperlens. *Nat Mater* **8**, 931–934 (2009).
15. Kildishev A V, Boltasseva A, Shalaev V M. Planar photonics with metasurfaces. *Science* **339**, 1232009 (2013).
16. Yu N F, Capasso F. Flat optics with designer metasurfaces. *Nat Mater* **13**, 139–150 (2014).
17. Ma G C, Yang M, Xiao S W, Yang Z Y, Sheng P. Acoustic metasurface with hybrid resonances. *Nat Mater* **13**, 873–878 (2014).
18. Luo X G. Subwavelength optical engineering with metasurface waves. *Adv Opt Mater* **6**, 1701201 (2018).
19. Pu M B, Feng Q, Wang M, Hu C G, Huang C *et al.* Ultrathin broadband nearly perfect absorber with symmetrical coherent illumination. *Opt Express* **20**, 2246–2254 (2012).
20. Li S C, Luo J, Anwar S, Li S, Lu W X *et al.* Broadband perfect absorption of ultrathin conductive films with coherent illumination: Superabsorption of microwave radiation. *Phys Rev B* **91**, 220301(R) (2015).
21. Pu M B, Hu C G, Huang C, Wang C T, Zhao Z Y *et al.* Investigation of Fano resonance in planar metamaterial with perturbed periodicity. *Opt Express* **21**, 992–1001 (2013).
22. Maa D-Y. Potential of microperforated panel absorber. *J Acoust Soc Am* **104**, 2861–2866 (1998).
23. Herdtle T, Bolton J S, Kim N N, Alexander J H, Gerdes R W. Transfer impedance of microperforated materials with tapered holes. *J Acoust Soc Am* **134**, 4752 (2013).
24. Qian Y J, Kong D Y, Liu S M, Sun S M, Zhao Z. Investigation on micro-perforated panel absorber with ultra-micro perforations. *Appl Acoust* **74**, 931–935 (2013).
25. Chambers B. Optimum design of a salisbury screen radar absorber. *Electron Lett* **30**, 1353–1354 (1994).
26. Knott E F, Langseth K. Performance degradation of Jaumann absorbers due to curvature. *IEEE Trans Antennas Propag* **28**,

137–139 (1980).

27. Duan Y T, Luo J, Wang G H, Hang Z H, Hou B *et al.* Theoretical requirements for broadband perfect absorption of acoustic waves by ultra-thin elastic meta-films. *Sci Rep* **5**, 12139 (2015).
28. Cheng Y, Zhou C, Yuan B G, Wu D J, Wei Q *et al.* Ultra-sparse metasurface for high reflection of low-frequency sound based on artificial Mie resonances. *Nat Mater* **14**, 1013–1019 (2015).
29. Smith F C. Design principles of broadband adaptive Salisbury screen absorber. *Electron Lett* **38**, 1052–1054 (2002).
30. Munk B A, Munk P, Pryor J. On designing Jaumann and circuit analog absorbers (CA absorbers) for oblique angle of incidence. *IEEE Trans Antennas Propag* **55**, 186–193 (2007).
31. Pu M B, Chen P, Wang Y Q, Zhao Z Y, Wang C T *et al.* Strong enhancement of light absorption and highly directive thermal emission in graphene. *Opt Express* **21**, 11618–11627 (2013).
32. Akselrod G M, Huang J N, Hoang T B, Bowen P T, Su L *et al.* Large-area metasurface perfect absorbers from visible to near-infrared. *Adv Mater* **27**, 8028–8034 (2015).
33. Chong Y D, Ge L, Cao H, Stone A D. Coherent perfect absorbers: time-reversed lasers. *Phys Rev Lett* **105**, 053901 (2010).
34. Pu M B, Feng Q, Hu C G, Luo X G. Perfect absorption of light by coherently induced plasmon hybridization in ultrathin metamaterial film. *Plasmonics* **7**, 733–738 (2012).
35. Li S C, Duan Q, Li S, Yin Q, Lu W X *et al.* Perfect electromagnetic absorption at one-atom-thick scale. *Appl Phys Lett* **107**, 181112 (2015).
36. Papaioannou M, Plum E, Valente J, Rogers E T F, Zheludev N I. Two-dimensional control of light with light on metasurfaces. *Light Sci Appl* **5**, e16070 (2016).
37. Li X, Pu M B, Wang Y Q, Ma X L, Li Y *et al.* Dynamic control of the extraordinary optical scattering in semicontinuous 2D metamaterials. *Adv Opt Mater* **4**, 659–663 (2016).
38. Rozanov K N. Ultimate thickness to bandwidth ratio of radar absorbers. *IEEE Trans Antennas Propag* **48**, 1230–1234 (2000).
39. Wang D C, Zhang L C, Gu Y H, Mehmood M Q, Gong Y D *et al.* Switchable ultrathin quarter-wave plate in terahertz using active phase-change metasurface. *Sci Rep* **5**, 15020 (2015).
40. Wan W J, Chong Y D, Ge L, Noh H, Stone A D *et al.* Time-reversed lasing and interferometric control of absorption. *Science* **331**, 889–892 (2011).
41. Wei P J, Croenne C, Chu S T, Li J. Symmetrical and anti-symmetrical coherent perfect absorption for acoustic waves. *Appl Phys Lett* **104**, 121902 (2014).
42. Zhang J F, MacDonald K F, Zheludev N I. Controlling light-with-light without nonlinearity. *Light Sci Appl* **1**, e18 (2012).
43. Ebbesen T W, Lezec H J, Ghaemi H F, Thio T, Wolff P A. Extraordinary optical transmission through sub-wavelength hole arrays. *Nature* **391**, 667–669 (1998).
44. Munk B A. *Frequency Selective Surfaces: Theory and Design* (Wiley, New York, 2000).
42. Han Y, Liu Y G, Huang W, Wang Z, Guo J Q *et al.* Generation of linearly polarized orbital angular momentum modes in a side-hole ring fiber with tunable topology numbers. *Opt express* **24**, 17272–17284 (2016).

Acknowledgements

We acknowledge the financial support by 973 Program of China under contract No. 2013CBA01700 and the National Natural Science Foundation of China under contract No. 61622509 and 61575203.

Competing interests

The authors declare no competing financial interests.